photonics

MDPI

Article

Uplink and Downlink NOMA Based on a Novel Interference Coefficient Estimation Strategy for Next-Generation Optical Wireless Networks

Syed Agha Hassnain Mohsan [1,2,†], Yanlong Li [2,3,4,†], Zejun Zhang [2], Amjad Ali [2] and Jing Xu [1,2,3,4,*]

[1] Donghai Laboratory, Zhoushan 316021, China; hassnainagha@zju.edu.cn
[2] Optical Communications Laboratory, Ocean College, Zhejiang University, Zhoushan 316021, China; lylong@zju.edu.cn (Y.L.); zhang-zj20@zju.edu.cn (Z.Z.); amjad@pku.edu.cn (A.A.)
[3] Ocean Research Center of Zhoushan, Zhejiang University, Zhoushan 316021, China
[4] Hainan Institute of Zhejiang University, Sanya 572025, China
* Correspondence: jxu-optics@zju.edu.cn
† These authors contributed equally to this work.

Abstract: Non-orthogonal multiple access (NOMA) has been widely recognized as a promising technology to improve the transmission capacity of wireless optical communication systems. NOMA considers the principle of successive interference cancellation (SIC) to separate a user's signal at the receiver side. To improve the ability of optical signal detection, we developed a quantum dot (QD) fluorescent concentrator incorporated with multiple-input and single-output (MISO) to realize an uplink NOMA-based optical wireless system. However, inaccurate interference assessment of multiple users using the SIC detection algorithm at the receiver side may lead to more prominent error propagation problems and affect the bit error rate (BER) performance of the system. This research aims to propose a novel recurrent neural network-based guided frequency interference coefficient estimation algorithm in a NOMA visible light communication (VLC) system. This algorithm can improve the accuracy of interference estimation compared with the traditional SIC detection algorithm by introducing interference coefficients. It provides a more accurate reconstruction possibility for level-by-level interference cancellation and weakens the influence of error propagation. In addition, we designed uplink and downlink NOMA-VLC communication systems for experimental validation. When the power allocation ratio was in the range of 0.8 to 0.97, the experimental results of the downlink validated that the BER performance of both users satisfied the forward error correction (FEC) limit with the least squares (LS)-SIC and the long short-term memory recurrent neural networks (LSTM)-SIC detection strategy. Moreover, the BER performance of the LSTM-SIC algorithm was better than that of the LS-SIC algorithm for all users when the power allocation ratio was in the range of 0.92 to 0.93. In particular, our proposed system offered a large detection area of 2 cm^2 and corresponding aggregate data rate up to 40 Mbps over 1.5 m of free space by using QDs, and we successfully achieved a mean bit error rate (BER) of 2.3×10^{-3} for the two users.

Keywords: non-orthogonal multiple access; successive interference cancellation; interference coefficient estimation; quantum dot; visible light communication; power allocation

check for updates

Citation: Mohsan, S.A.H.; Li, Y.; Zhang, Z.; Ali, A.; Xu, J. Uplink and Downlink NOMA Based on a Novel Interference Coefficient Estimation Strategy for Next-Generation Optical Wireless Networks. *Photonics* **2023**, *10*, 569. https://doi.org/10.3390/photonics10050569

Received: 14 April 2023
Revised: 9 May 2023
Accepted: 10 May 2023
Published: 12 May 2023

Copyright: © 2023 by the authors. Licensee MDPI, Basel, Switzerland. This article is an open access article distributed under the terms and conditions of the Creative Commons Attribution (CC BY) license (https://creativecommons.org/licenses/by/4.0/).

1. Introduction

Visible light communication (VLC) is deemed to be an efficacious candidate for high data rate communication and efficient ubiquitous connectivity, and a remarkable complement to traditional radio frequency (RF) communication. It has the capability to overcome the spectrum scarcity and capacity limitation of RF communication. VLC offers several promising features such as an unlicensed spectrum, low implementation cost, low power consumption, high transmission rate, high confidentiality, relatively low health hazards, and immunity to interference from electromagnetic radiation. With the increasing inherent

drawbacks of RF spectrum congestion and the unprecedented demand for high-speed communication, VLC can provide a high-speed and large-capacity solution for indoor wireless communication networks and is considered to a wireless communication technology with inevitable application prospects. It offers several unique transmission capabilities making it feasible in various scenarios, such as visible light positioning (VLP) [1], optical camera communication [2,3], underwater communication [4–7], free-space optical communication (FSO) [8,9], and integrated lighting and communication [10]. Efficient transmission is the key point to communication system design. Traditional RF communication is based on fixed resource allocation by orthogonal allocation of the time, frequency, and code domains of the system [11,12], which makes users communicate independently of the resources and do not interfere with each other. The latest wireless optical code division multiple access technology has also been studied and implemented [13,14]. However, the number of nodes that can be served by an orthogonal multiple access system at the same moment cannot exceed the number of orthogonal resources; therefore, the system throughput performance is limited. In order to meet the diverse and stringent transmission needs in the envisioned indoor intelligent network transmission, it is necessary to study the access resource allocation for VLC access systems. Indoor optical access is significantly different from the multiple access technology of RF communication due to the limited radiation distance and angle range. Therefore, it is important to use its directional radiation to form a beam for indoor multiple optical access. In [15], the new non-orthogonal multiple access (NOMA) was reported for indoor environments for multi-user downlink communication by taking advantage of light intensity distribution or uneven transmission distance without frequency and time conflicts.

Thus, this key distinguishing feature makes it a promising approach for single-receiver multiple-input and multiple-output (MIMO) VLC in an uplink system [16]. The authors proposed a NOMA scheme incorporated with orthogonal frequency division multiplexing access (OFDMA) for VLC, which provided a high system capacity, flexible bandwidth, and high throughput for a large number of users [16]. The results indicated that inter-user interference could be effectively eliminated through accurate channel estimation. In order to experimentally realize a MISO system, one key constraint is étendue conservation. Increasing the active area of the photodetector receiver can significantly enhance the signal-to-noise-ratio (SNR), but it also raises the concern of lower data rate due to limited bandwidth. A traditional approach to enhance the SNR is to focus light through optical lenses. However, these optical concentrators are usually constrained by the conservation of étendue, resulting in a tradeoff between field-of-view (FoV) and optical gain [17]. Hence, the fluorophore, which initially absorbs impingent light and then re-emits it at a longer wavelength, is designed to overcome the above shortcoming. Both single and double fluorescent layers have been considered as concentrators to attain high gain and wide FoV in VLC systems [18,19]. Moreover, the authors in [20] proposed a nanopatterned fluorophore on a flexible matrix to achieve higher optical gain without affecting the FoV. They developed nanopatterned luminescent solar concentrators (LSCs) as VLC detectors to double the optical gain compared to conventional rectangular counterparts. This was also proposed to expand the receiving spectral range of conventional silicon (Si) photodetectors for high-speed solar-blind ultra-violet (UV) communication [21]. It validated the feasibility of a high-speed photoreceiver structure with a composition-tunable perovskite-based phosphor and a low-cost Si-based photodetector. Because of its wide FoV, the authors in [22] used a novel fluorescent concentrator in a 2×2 MIMO indoor VLC system providing a corresponding data rate of 32 Mbps through conventional on–off keying (OOK). It potentially enabled a high degree of spatial multiplexing to be attained through a simple receiver design with a wide FoV. However, most of the MIMO systems have limited data rates of 10–40 Mbps due to narrow bandwidths and low SNRs.

In addition, multiple access technologies are classified into two categories, namely, orthogonal multiple access (OMA) and NOMA, according to different methods of resource division. NOMA technology divides time, code, and power dimensional resources in

a non-orthogonal way. The resources are used to carry out data bearing-transmission, which can support flexible connectivity and allow for more efficient use with limited resources [23,24]. To guarantee the effective utilization of resources and enhanced capacity of the access system, the NOMA-VLC system is designed in uplink and downlink data transmission. It can also offer several other enticing merits, such as high spectral efficiency, low transmission latency, and fast access with few interactions. However, there are certain challenges that limit the performance of NOMA-VLC systems such as the error propagation issue together with the nonlinear distortion caused by limited modulation bandwidth, multipath effect, and nonlinearity of optical sources, e.g., light-emitting diodes (LEDs). Moreover, securing accurate channel state information, which is essential to recover the non-orthogonally synthesized signal, is also challenging in NOMA-VLC systems. NOMA systems utilize the sophisticated successive interference cancellation (SIC) technique at the receiver side for data detection and multiple access interference suppression [25], which makes it possible to transmit information from multiple users overlapping on the same resource unit simultaneously. However, the multi-user data detection problem is a bottleneck for its further performance improvement.

NOMA-VLC systems are prone to two major drawbacks, which are (i) availability of the line-of-sight (LOS) link, and (ii) overall complexity and overhead of the feedback mechanism involving channel quality. The drawback of the LOS link usually arises in VLC systems with mobile users due to random receiver orientations, which is highlighted in [26–28]. A novel metric for the access point adoption problem has been investigated for receivers with random orientations [29]. For a downlink VLC system, the handover issue is discussed in [30], where device rotation is kept into consideration to compute the handover probability. A generic mechanism for the random receiver orientation is designed in [31], where the square-channel gain distribution is computed analytically. The proposed mechanism applies to any prior distribution for the receiver orientation, which is further developed for multi-LED scenarios in [26]. The effect of titling the receiver angle on the BER performance is investigated in [32]. To overcome the challenge of the LOS link, a potential solution is to use QDs with wide FoVs, which is the key motivation of our work.

In [33], a joint detection method using phase pre-distortion for multi-user detection in a NOMA-VLC system was proposed, which had acceptable pre-distortion effects at low, medium, and high SNR, better than the interference cancellation detection algorithm. In [34], symmetric superposition coding and symmetric successive interference cancellation decoding techniques were implemented, and the effectiveness was experimentally verified, which eliminated 90% of the demodulation error compared to the conventional orthogonal multiple access system. The aforementioned methods investigated NOMA techniques based on power or code domain resources and did not consider NOMA techniques under multidimensional resource multiplexing. Additionally, these methods cannot solve the problem of multi-user detection under multidimensional resources.

One crucial challenge is how to allocate power to NOMA users when there are limited resources. The power allocation to each user is performed in a sophisticated manner in order to prevent a specific user from accumulating the total power. It has a substantial impact on the performance of the NOMA technique, such as interference management and rate distribution among users. The performance of NOMA schemes strongly depends on the power allocation, where inaccurate power allocation can cause interference among superimposed users [35]. Consequently, it will degrade the BER performance, rate distribution, and outage of NOMA users. Interference between the NOMA users can be avoided by choosing power allocation accurately. An appropriate power allocation with low complexity is highly desirable to exploit the power domain optimally in practical NOMA-based VLC systems. Power allocation is important in NOMA systems to improve the system throughout, spectral efficiency, energy efficiency, capacity, quality of service (QoS), and user fairness. Moreover, accurate power allocation and an appropriate user pairing technique [36] must be compatible to achieve better performance of NOMA systems. Important parameters that are required to design power allocation schemes are total power constraint,

QoS requirements, maximizing objective function, channel conditions, CSI availability, and many more. Some of the performance metrics used for power allocation schemes are the number of admissible users, energy efficiency (EE), SNR, channel gain, fairness index, and sum rate [37].

An energy efficient NOMA scheme for bidirectional VLC systems was proposed in [38] to maximize energy efficiency under certain QoS targets through an optimal power allocation approach. At present, although many studies have applied NOMA technology in optical communication systems, the power allocation and the SIC signal detection technology of NOMA have not been thoroughly studied, and the error propagation problem is more prominent. In [39], the challenges faced by introducing a NOMA-VLC system were summarized, including power allocation, how to combine it with optical orthogonal frequency-division multiplexing (OFDM) modulation, and how to combine it with multiple-input multiple-output (MIMO). In [40], a gain ratio power allocation (GRPA) strategy was proposed to allocate power to individual users according to their channel status, which improved the effectiveness and fairness of the system. In [41], a power allocation scheme based on GRPA was introduced with a look-up table method. The system complexity was reduced by designing a channel gain table for power allocation. In [42], the NOMA technique was introduced into the MIMO multi-user VLC system. For the characteristics of MIMO technology, the paper proposed a normalized gain difference power allocation (NGDPA) method to improve the system capacity and transmission efficiency. A summary of recent works on NOMA systems is provided in Table 1.

Table 1. Summary of recent studies on NOMA systems.

Reference	Communication Domain	Focus Area
[43]	VLC	Karush–Kuhn–Tucker (KKT) optimality conditions to enhance sum-rate performance over that of OFDMA
[44]	VLC	Convex optimization applied to improve data rate of downlink NOMA-VLC
[45]	VLC	Iterative algorithm to attain an additional sum-rate gain of 10 Mbps for NOMA users compared to time division multiple access (TDMA)
[46]	VLC	Harris Hawks optimization to enhance sum-rate performance by jointly optimizing power allocation and placement of unmanned aerial vehicle (UAV)
[47]	VLC	Gradient projection (GP) algorithm to gain higher sum-rate performance than OMA
[48]	VLC	Interior point approach and zero forcing (ZF) pre-coding-based NOMA techniques outperform traditional NOMA and ZF
[49]	VLC	Energy-efficient power allocation (EPA) technique to improve energy efficiency of NOMA-based IoT networks
[50]	VLC	Power allocation and user pairing approaches for downlink VLC-NOMA
[51]	VLC	Analytical method and power allocation method for better maximum sum-rate than fixed power allocation (FPA) and GRPA
[52]	VLC	KKT optimality conditions to attain higher system sum-rate than FPA and NGDPA
[53]	Hybrid OMA and NOMA VLC	Dynamic programming-based layer-recursion model for better achievability throughput than traditional NOMA and TDMA
[54]	RF communication	Distance-dependent power allocation (DDPA) technique for mMIMO-aided NOMA
[55]	RF communication	Energy-efficient power allocation for multiple-user MIMO-NOMA
[56]	RF communication	Power allocation to ensure QoS requirements in NOMA systems
[57]	RF communication	Power allocation to ensure individual QoS requirements in downlink NOMA systems
[58]	RF communication	Binary continuous phase modulation (CPM) with modulation is considered into downlink symbol-asynchronous non-orthogonal multiple access (ANOMA) to improve spectral and power efficiency
[59]	Hybrid RF/FSO	Superior performance of FSO backhauling for high-reliability and high-throughput NOMA systems compared to RF backhauling
[60]	Hybrid RF/FSO	Superior outage performance for an FSO-RF system with NOMA under a dual energy harvesting (EH) mode compared to single EH mode
[61]	Hybrid RF/VLC	Link selection and user pairing in cooperative-NOMA
[62]	Hybrid RF/VLC	Outage performance and reliability improvement of cooperative-NOMA

In this paper, an optical NOMA communication system with a new SIC signal detection receiver was constructed to address the above problems. A novel successive interference cancellation detection algorithm was proposed to improve the accuracy of interference estimation by introducing interference coefficients in the optical NOMA system. Furthermore, the method of collecting light based on a fluorescent concentrator was used to improve the light collection efficiency in the uplink optical NOMA system. Moreover, a recurrent neural network-based guided frequency interference coefficient estimation algorithm was proposed to provide a more accurate reconstruction possibility for the level-by-level interference cancellation and improve the bit error rate (BER) performance of the downlink optical NOMA system for multiple users.

2. NOMA System Model

2.1. System Design

As shown in Figure 1, an indoor NOMA-VLC system uses the SIC technique in both uplink and downlink data detection, for which the interference coefficient is precisely estimated. In the indoor environment, with the uplink NOMA system in the lower left corner, User 1 and User 2 use NOMA power allocation coding to transmit signals to the receiver. The receiver uses SIC detection technology after photoelectric detection to sort users according to their distance to the transmitter and performs interference cancellation detection. In the lower right corner is the downlink NOMA-VLC system, where the transmitter adjusts the transmitting power in the electrical domain according to the location of the receiving users, such that different users receive different optical powers. The SIC detection method presented in this paper is suitable for signal detection of indoor uplink and downlink data transmission scenarios. The difference is that the uplink NOMA only requires the base station to have an SIC receiver, while the downlink NOMA requires each user to have an SIC receiver.

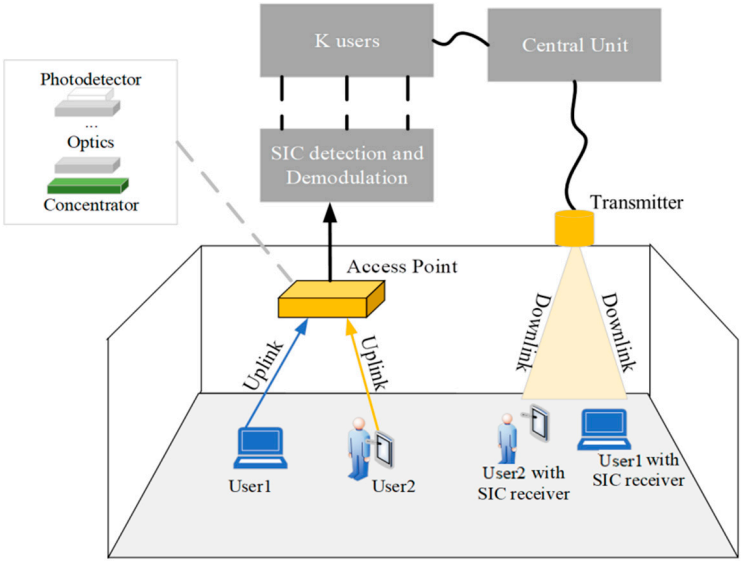


Figure 1. Indoor optical communication scene diagram.

2.2. Uplink NOMA

The uplink NOMA requires signal aggregation. In order to successfully implement the aforementioned architecture, we experimentally demonstrated a 2×1 MISO system enabled by the QD concentrator. Since the signals come from different directions, the photodetector suffers from relatively low energy efficiency and a narrow FoV, and the introduction of a QD concentrator can improve the energy conversion efficiency as well as the FoV. In our experimental demonstration of the uplink NOMA, we used two different QDs and compared their BER performance for two users. Both QDs varied in terms of characteristics and optical performance. For instance, the full widths at half maximum

of QD Material-1 (CdSe/ZnS) and QD Material-2 ($CsPbBr_3$-50) were 26 nm and 18 nm with central emission wavelengths of 526 nm and 514 nm, respectively. In order to further calculate the frequency response in QD-converted exciting light, first we needed to measure the photoluminescence (PL) lifetime of each material. The photoluminescence (PL) lifetime of CdSe/ZnS and CsPbBr3-50 were determined to be 32 ns and 29 ns, respectively. We collected the time-resolved PL lifetime of QDs at 526 nm and 514 nm, respectively, which was comparable to the lifetime of other inorganic color converters, ensuring potential use for hundreds of Mbps VLC [17]. The photoluminescence quantum yield was 86% at 450 nm for Material-1 and 80% at 450 nm for Material-2, which was high enough to support optical gain. The different characteristics and optical performance of the two quantum dots used in our experiments are provided in Tables 2 and 3, respectively.

Table 2. Characteristics of quantum dot Material-1 (CdSe/ZnS) and Material-2 ($CsPbBr_3$-50).

Characteristics	Material-1	Material-2
Volatile substances (toluene)	99.65 wt%	96.51 wt%
Non-volatile organics	0.06 wt%	0.85 wt%
Inorganics	(QD CdSe/ZnS) 0.29 wt%	(QD $CsPbBr_3$) 2.64 wt%
Density	0.870 g/cm^3	0.867 g/cm^3
QD (inorganics + ligands) Con.	3 mg/mL	3 mg/mL

Table 3. Optical performance of quantum dot Material-1 (CdSe/ZnS) and Material-2 ($CsPbBr_3$-50).

Optical Performance	Material-1	Material-2
PL peak emission wavelength	526 nm	514 nm
Full wave at half maximum	26 nm	18 nm
Photoluminescence quantum yield	86%	80%

The absorption and emission spectra of QDs (Material-1, CdSe/ZnS) are shown in Figure 2a,b. The transmission electron microscopy (TEM) images of the QDs at different scales are provided in Figure 2c,d, which clearly indicate uniform core–shell QD particles with an average size of 7.2 nm.

Similarly, the absorption and emission spectra of QDs (Material-2, $CsPbBr_3$-50) are shown in Figure 3a,b. The TEM images of the QDs at different scales are provided in Figure 3c,d, which clearly indicate uniform core–shell QD particles with an average size of 9.8 nm.

2.3. Downlink NOMA

In the downlink NOMA-VLC system, this paper mainly considers a single-cell downlink scenario with one base station and N users, $U_i, i = 1, 2, 3, \ldots, N$, and all terminals are equipped with a single optical antenna. It is worth noting that there is a similar case for the uplink scenario. For users with weak channel conditions, a higher power is allocated for the sending signal, while the contrary is the case for users with better channel conditions. At the transmitter end, the base station communicates with all users through the same time–frequency resource and different powers. At the receiving end, reception is performed through SIC. When the SIC receiver demodulates the signal of a NOMA user, it detects and removes the signals of other NOMA users with higher power and considers the users with lower power as interference. In particular, a receiving user with optimal channel conditions eliminates the signal of all other NOMA users when demodulating its own signal.

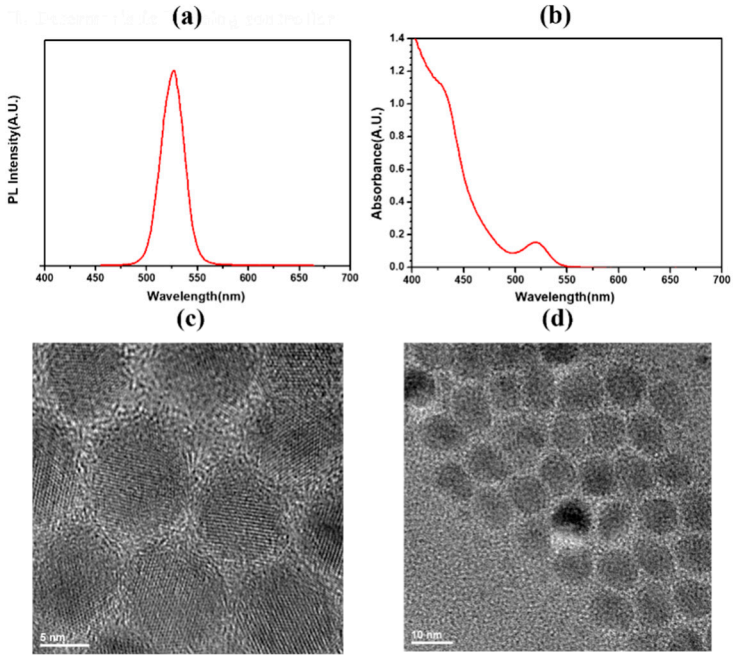


Figure 2. Material-1: (**a**) normalized excitation spectra of QDs, (**b**) normalized emission spectra of QDs, (**c**) TEM, and (**d**) high-resolution TEM images of the QD material.

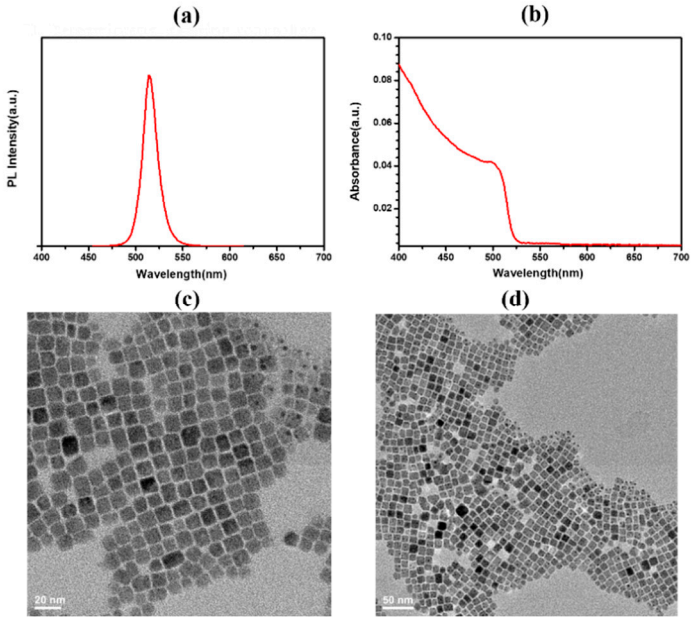


Figure 3. Material-2: (**a**) normalized excitation spectra of QDs, (**b**) normalized emission spectra of QDs, (**c**) TEM, and (**d**) high-resolution TEM images of the QD material.

In practice, interference reconstruction is complicated in the SIC detection for multiple users. The transmitter assigns higher power P_1 to the first user's signal x_1, and it assigns lower power P_2 to the second user's signal x_2. In this case, the power allocation factor can be expressed as $\frac{P_1}{P_1+P_2}$. Then the transmitter superimposes both signals and transmits them simultaneously. h_i is the channel gain for an optical communication system. The superimposed signal s can be expressed as

$$s = \sqrt{P_1}x_1 + \sqrt{P_2}x_2 \tag{1}$$

The total signal y_i $(i = 1, 2)$ can be expressed as the sum of the received signal and the channel Gaussian white noise w_i:

$$y_i = h_i s + w_i \tag{2}$$

Moreover, we calculate the theoretical capacity for the strong and weak users of the NOMA system according to Equation (3). We consider the normalized bandwidth to be 1. As shown in Figure 4, the capacity of the strong user (R_1) is higher than that of the weak user (R_2) for the downlink NOMA system.

$$R_1 = \log_2(1 + \frac{P_1|h_1|^2}{w_1}),\ R_2 = \log_2(1 + \frac{P_2|h_2|^2}{P_1|h_2|^2 + w_2}) \tag{3}$$

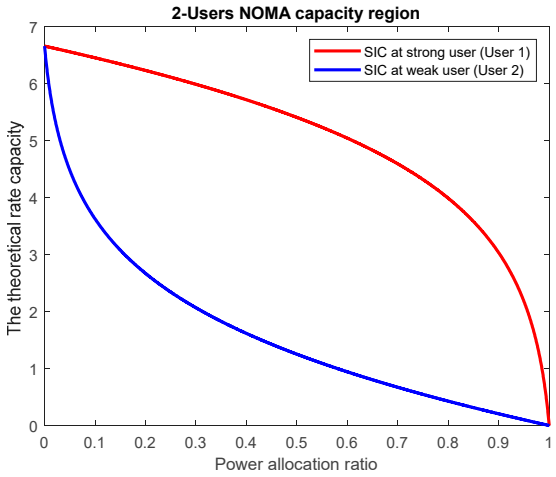


Figure 4. Downlink 2-user NOMA capacity region.

Considering a NOMA system with two users, the signal with higher power is x_2, so the first output is x_2 by direct detecting. The signal estimate of x_2 is recovered, and it is subtracted from the received signal y. Then, the second output x_1 is demodulated. Thus, the user with weak power needs to demodulate the signal twice [63]. Using such a detection sequence, it can realize the multiplexing of two signals in the power domain. As shown in Figure 4, the capacity of the strong user is higher than that of the weak user due to the different power allocations according to Shannon's theorem, but the relative capacity performance of weak user is also guaranteed.

A key point in the SIC signal detection process is the user detection order. Here, the sequencing is performed based on the signal power of the users. In NOMA systems with more than two users, the transmitter will use power multiplexing techniques to allocate power to different users. Usually, users with high channel gain are allocated low power, while users with low channel gain are allocated high power. When the synthetic NOMA signal reaches the receiver, the signal power of each user will be different, and the SIC receiver will sort out the users according to their signal power and demodulate the different signals for each user accordingly. It can achieve the purpose of differentiating users in the NOMA system [64].

Compared with the traditional SIC receiver, the SIC receiver used in NOMA is more complex and requires a stronger signal processing capability. In actual signal processing, the power of users is constantly changing, which requires the SIC receiver to constantly rank the user power. As seen in the SIC structure diagram, each level of processing generates a certain time delay, and in real multi-level signal processing, the generated time delay is large [65]. In level-by-level interference removal, the accuracy of interference reconstruction in the previous level affects the demodulation of the signal in the later level [66]. Generally, the solution of the delay of real multi-level signal processing depends on the

future improvement of chip processing capability, while the level-by-level interference removal detection requires further research on the related processing algorithms.

In this paper, we propose to implement a training sequence and estimation algorithm to improve the accuracy of interference estimation. In order to obtain the accurate interference caused by the artificially introduced interference and bandwidth-limited devices in each part of the system, we perform full-signal fading estimation.

3. SIC Detection Based on Interference Estimation Coefficient

As shown in Figure 5, the signals of User 1 and User 2 are encoded in the power domain by the base station, and the users use a SIC receiver to detect their own signals. The traditional SIC detection algorithm, which directly carries out interference reconstruction, does not consider the nonlinear effect of the device. In this paper, the interference coefficient was firstly introduced to further accurately estimate the interference and reduce the error propagation. The interference coefficient was estimated by regression using the least squares (LS) and long short-term memory recurrent neural networks (LSTM) algorithms. We used β to describe the interference estimation coefficient in this paper.

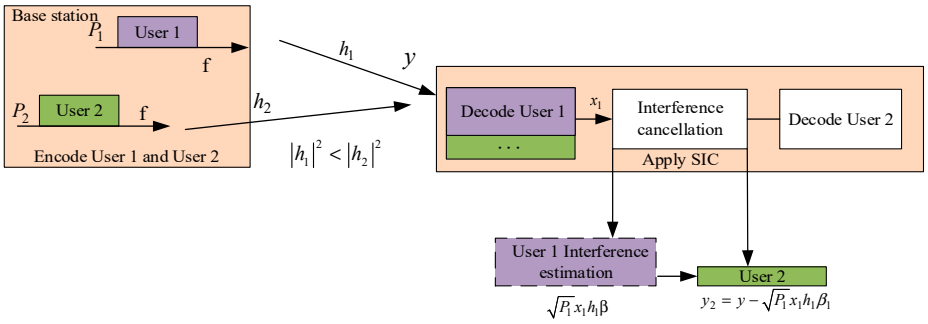


Figure 5. SIC schematic block diagram.

As shown in Figure 5, the two users are assigned different transmitting powers. The user with low channel gain is assigned a high transmitting power, and the superimposed signal is transmitted by the base station. As User 1 has a low channel gain, high power is allocated to User 1, and the signal is detected directly. The high power of User 1 leads to strong interference for User 2, so it is necessary to estimate the interference of User 1 to User 2. Next, we discuss how to estimate the interference coefficient to reconstruct the signal of User 1 for User 2 detection.

Proposed Algorithm

The expression for the interference cancellation process is given as Equation (4). To obtain accurate interference, the interference estimation coefficient β is introduced to modify the estimated interference. Here, h_i is the channel gain for the optical communication system, and $\sqrt{P_1}x_1h_1\beta$ is used to represent the interference. After recovering the interference estimate of x_2 and subtracting it from the received signal y, the received y_2 for the second user is obtained as Equation (4). In order to obtain β, we used the training sequence inserted in the first total frame. The training sequence is not required for the later data frame. Specifically, β can be estimated by the LS or LSTM algorithm with the training sequence.

$$y_2 = y - \sqrt{P_1}x_1h_1\beta \tag{4}$$

The interference estimation coefficient is calculated as Equation (5) by the LS algorithm.

$$\beta = (\mathrm{X}^{\mathrm{T}}\mathrm{X})^{-1}\mathrm{X}^{\mathrm{T}}\mathrm{y} \tag{5}$$

Here, X represents the transmitting signal. Since the LS estimation algorithm needs all training sequences of one frame to calculate the interference estimation coefficient, the cost is too high in this process. For an accurate estimation, the LSTM algorithm is introduced

for interference coefficient estimation of the whole NOMA-VLC system [67–69]. As shown in Figure 6, LSTM is a special kind of recurrent neural network that is capable of learning long dependencies. Therefore, the LSTM-SIC algorithm is proposed based on the recurrent neural network, which uses the first 12 training sequences within a frame to forecast the following 3 interference estimation coefficients. The interference coefficient can be obtained by LSTM to reconstruct interference signal and substantially reduce the overhead of the training sequence.

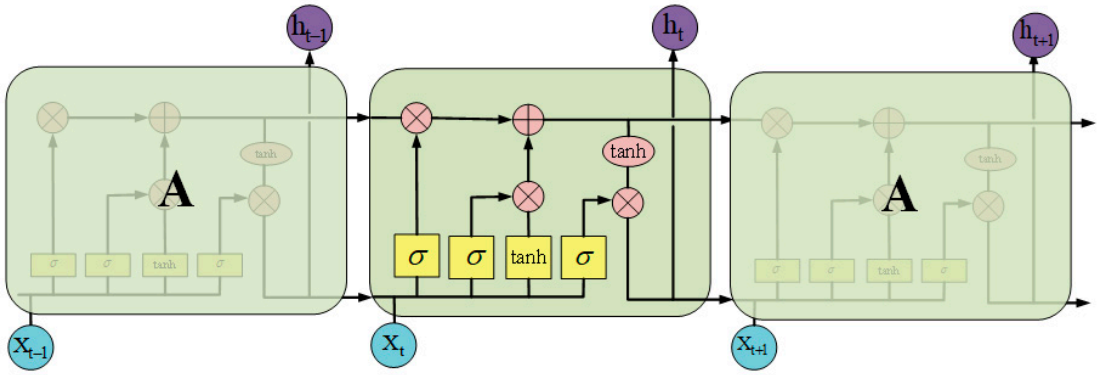


Figure 6. Four interacting neural network layers in the repetition module of the LSTM.

As shown in Figure 7, the LSTM algorithm can be used to predict the interference coefficient. It can be seen that after neural network prediction training, the predicted value and the real value tended to be the same, as seen in Figure 8a, and the cumulative error function of the prediction network converged well after iteration, as seen in Figure 8b.

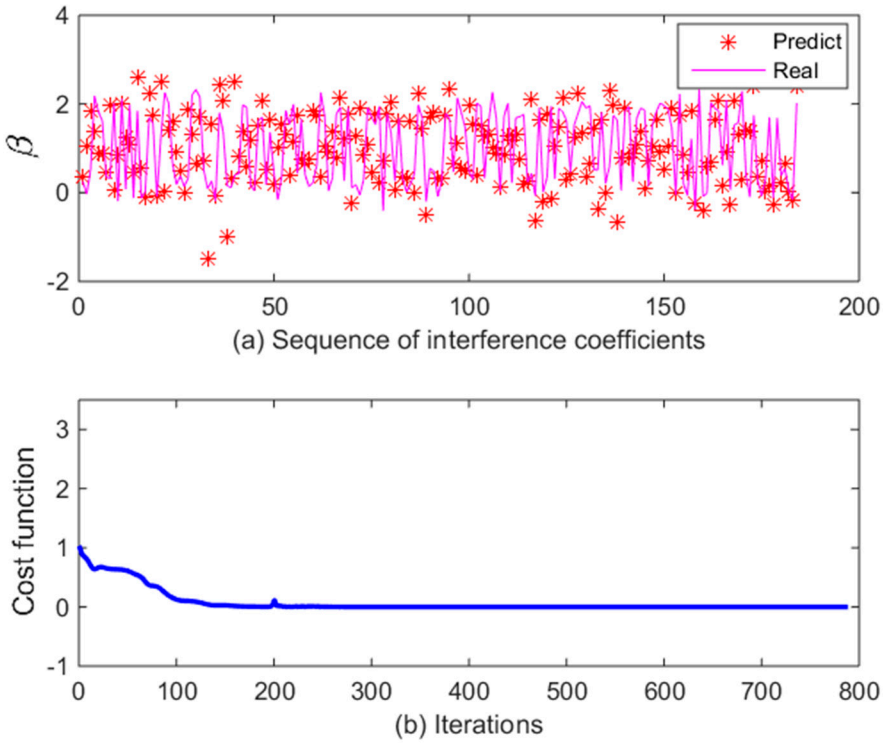
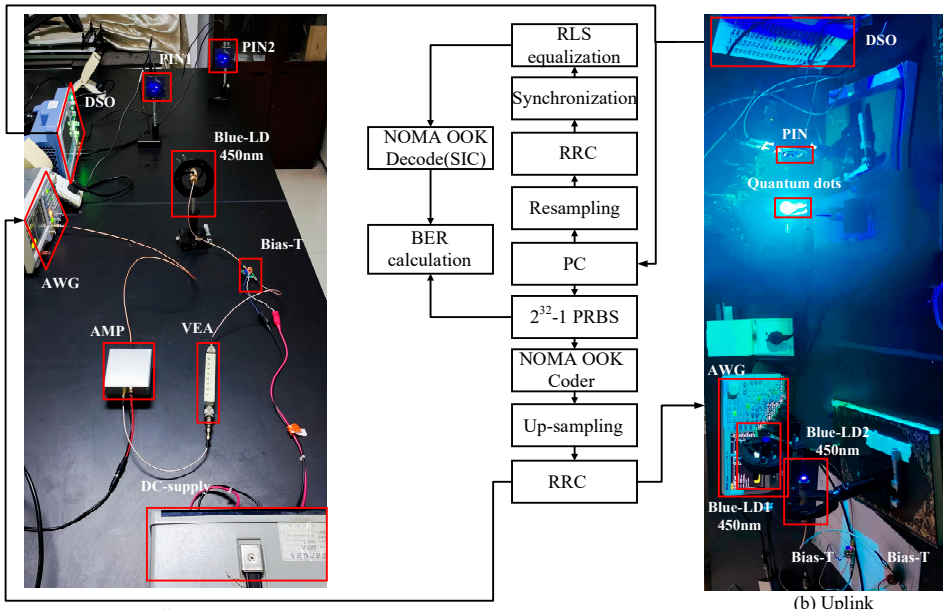


Figure 7. Prediction results of training of interference coefficient.



(a) Downlink NOMA-VLC

(b) Uplink NOMA-VLC

Figure 8. Blocks diagrams of the experimental setup: (**a**) block diagram of downlink NOMA-VLC using LSTM SIC receivers; (**b**) block diagram of uplink NOMA-VLC using quantum dots.

4. Experiments and Analysis of Results

To realize this work, the experimental system is shown in Figure 8. Firstly, based on the SIC interference detection algorithm described in the previous section, the relevant device performance was tested. Secondly, the BER performance of the NOMA signal synthesized from two 20 Mbps OOK signals under different powers was analyzed. The BER performance of the NOMA-VLC system with different power allocation ratios, bias currents, and signal amplitudes are optimized.

The block diagram of the experimental setup is shown in Figure 8a. First, two pseudo-random bit sequences of length 2^{32}-1 were generated offline at the PC, followed by OOK modulation and superposition coding of the two sequences in the power domain to generate the NOMA OOK signal. It was further up-sampled and processed via a raised root cosine filter (RRC) before loading into an arbitrary waveform generator (AWG). The output signal passed through an amplifier (AMP) and a variable electrical attenuator (VEA), and then it passed through a T-shaped bias (Bias-T) to drive a blue LD. The optical signal emitted from the LD passed through the wireless channel. At the receiving end, the optical signal was detected by a 125-MHz PIN photodetector at different locations, where the PIN photodetector worked as different users' receiver. The signal was captured by a mixed-signal oscilloscope (MSO), which subsequently sent the signal to the PC for off-line processing, including resampling, RRC, timer synchronization, recursive least squares (RLS) equalization, and NOMA OOK demodulation. Finally, the system BER was calculated.

Figure 8b represents the entire system based on blue laser diodes with a 1.5 m horizontal free-space transmission distance. Two NOMA signals were generated using an AWG and transmitted by two calibrated blue LDs of 450 nm. LD1 and LD2 were separated by 0.5 m. At the receiving end, we used QD thin film to capture two optical beams and then pass it through a single PIN to realize signal reception at DSO. The modulated blue laser beams were incident on the QD concentrator, fully overlapping each other. We precisely adjusted the position of the QD film to achieve concentrator-to-detector coupling over a short distance. After passing the blue light from the QD film, the generated green light from QD was collected by a 125 MHz PIN photodetector receiver. Next, we used offline MATLAB processing to successfully decode both signals. Furthermore, we divided the experiment

process into two parts: one was the performance test for the uplink NOMA-VLC system, and the other was the performance test for the downlink NOMA-VLC system.

In this experiment, the P–I and V–I curves of the LD are illustrated in Figure 9. In the operating range, with the increase of current, the output power and output voltage increased, and there was a linear region from 0.2 to 0.8 A.

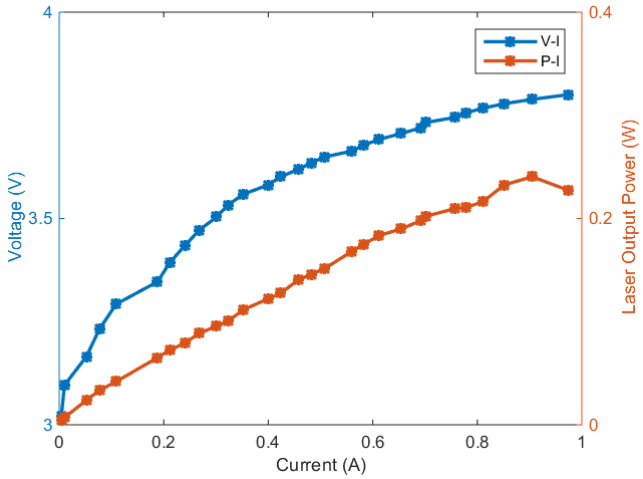


Figure 9. P–I and V–I measurement results.

4.1. The Analysis of Uplink NOMA-VLC

In the uplink NOMA-VLC system, the BER performance for different bias currents, attenuation values, and power allocations were analyzed. Figure 10 represents the BER performance of User 1 and User 2 with different bias current values. It can be seen that the BER performance of all users with Material-2 was below the forward error correction (FEC) limit criterion when the bias current was 0.6 A. As the bias current increased from 0.1 to 0.6 A, the BERs of all users with Material-1 and Material-2 showed decay. The BERs of all users with both materials increased when the bias current increased from 0.6 A to 1 A. Therefore, in our following experiment, the bias current value was set to 0.6 A to obtain the best BER performance.

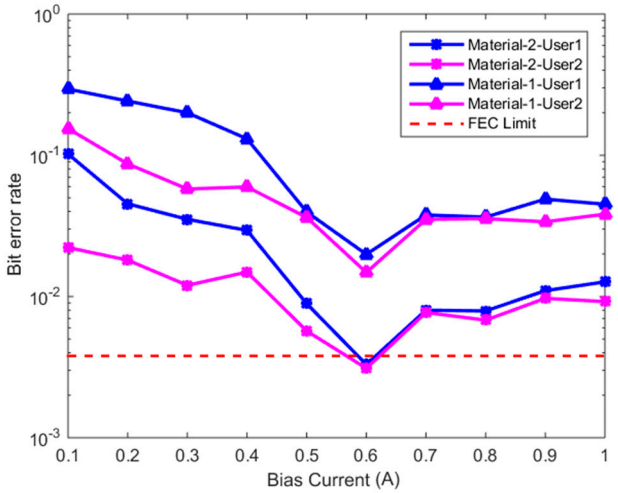


Figure 10. BER performance of NOMA-VLC under different bias current values.

Figure 11 shows the BER performance of User 1 and User 2 for uplink NOMA-VLC with Material-1 and Material-2 considering different attenuation values. As the attenuation increased, the BERs of all users showcased a decay. We executed various experimental trials to achieve an optimized attenuation of 10 dB to find out the best conceivable BER

performance. As we increased the attenuation above 10 dB, all the BERs indicated a rise in each associated curve. Next, we used the LS-SIC algorithm to further improve the BER performance. It is worth noting that the BER performance of both users considering both materials was below the FEC limit criterion while using the LS-SIC algorithm when the attenuation was 10 dB.

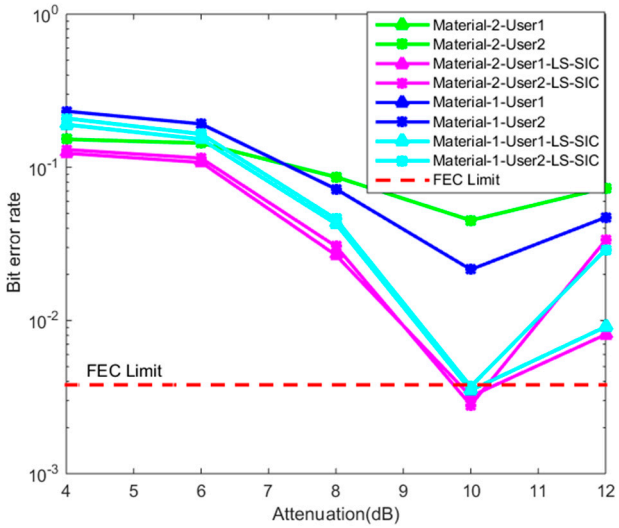


Figure 11. BER performance of NOMA-VLC under different attenuation values.

In order to secure successful signal decoding, there must be a sufficient power difference between received signals. We used the optimized values of bias current and attenuation and the control power allocation ratio in the NOMA system to obtain multiplexing transmission. Figure 12 shows the BER performance for two users considering different power allocation ratios. For experimental demonstration, we considered power allocation ratios to be 0.90, 0.91, 0.92, 0.93, 0.94, 0.95, 0.96, and 0.97. The decreasing exponential curves showed that a higher power allocation ratio was suitable for better BER performance. We noticed that the best BER performance was obtained at the power allocation ratio of 0.96. Moreover, our findings indicated that the MISO-NOMA-VLC system could support an aggregate data rate of 40 Mbps within the FEC criterion in the uplink NOMA-VLC system.

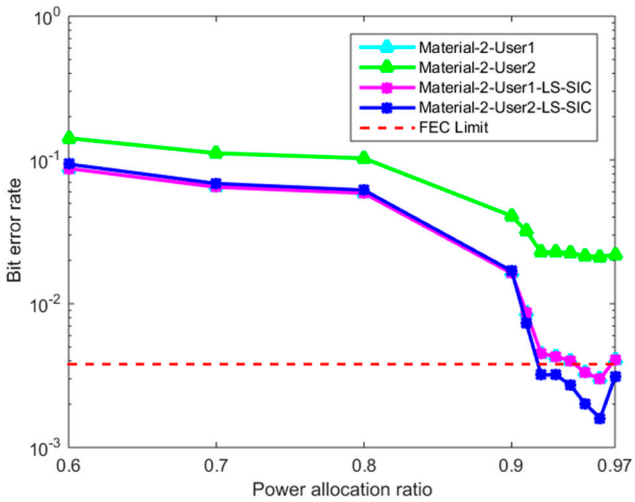


Figure 12. BER performance of two users with Material-2 for various power allocation ratios.

4.2. The Analysis of Downlink NOMA-VLC

In the downlink NOMA-VLC system, the BER performance for different bias currents, attenuation values, and power allocations was analyzed. It can be seen from Figure 13 that

with the various bias current values, the BER increased, and the optimal value was obtained at 0.22 A. When the attenuation value was set from 2 to 11 dB, a higher attenuation value led to better BER performance, and the best BER performance was obtained at 11 dB.

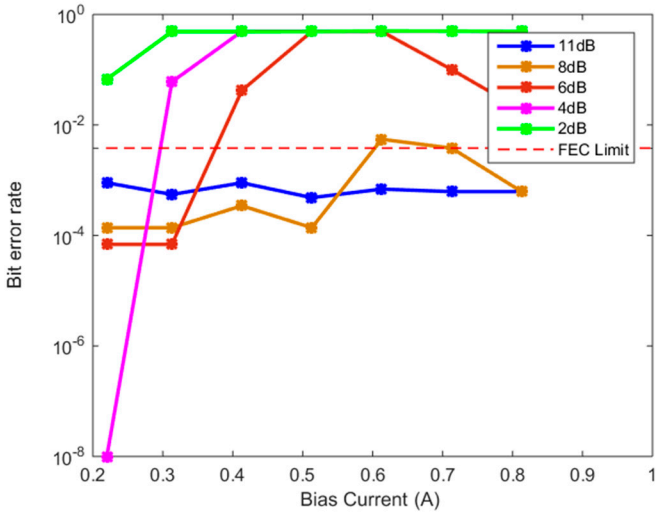


Figure 13. Original BER curve without interference estimation optimization.

Figure 14 shows the BER performance of the NOMA-OOK system for different distance variations with LS-SIC and LSTM-SIC detection algorithms under the conditions of optimal bias current and attenuation values. It can be seen that the traditional SIC, LS-SIC, and LSTM-SIC detection algorithms changed the BER at different distances for each user. Since the power allocation of the two users was different, the signal of strong user was detected directly with a low level of interference. However, when the weak user was detected, the BER performance sharply deteriorated with the elimination of more interference of the strong user inaccurately. Therefore, the BER of User 1 was better than that of User 2. However, after introducing interference estimation coefficients to accurately reconstruct the interference, the BER performance of User 2 became better. Furthermore, when the transmission distance was less than 5.5 m, the BERs of both users were lower than the FEC limit when using LS-SIC and LSTM-SIC detection algorithms. As the distance continued to increase to 7.5 m, the BERs of User 1 with both algorithms were still lower than the FEC limit, while the BERs of User 2 were lower than the FEC limit when the distance was within 6 m. When the distance exceeded 6 m, the BER of User 2 with the LS-SIC algorithm was higher than the FEC limit, while the BER with the LSTM-SIC algorithm was still lower than the FEC limit up to 7.5 m. Therefore, the interference estimation performance was optimized by using the LSTM to estimate the interference coefficient with the training sequence.

In addition, insets are the eye diagrams (a, b, c, d) for the corresponding BERs indicated by the arrows. The eye diagram of User 1 with equalization is represented by (a). The open eyes indicate that this signal is suitable for demodulation. The eye diagram of User 2 with equalization is represented by (b). We can see that the eyes are invisible, which indicates the signal is not suitable for demodulation. Next, we used the LS-SIC algorithm to improve the quality of User 2, as shown in eye diagram (c). Here, the open eyes indicate the performance improvement. We also considered LSTM-SIC to further improve the performance of User 2, as shown in eye diagram (d). We can clearly see that the eyes are wide open, resulting in better performance, and the signal is suitable for demodulation.

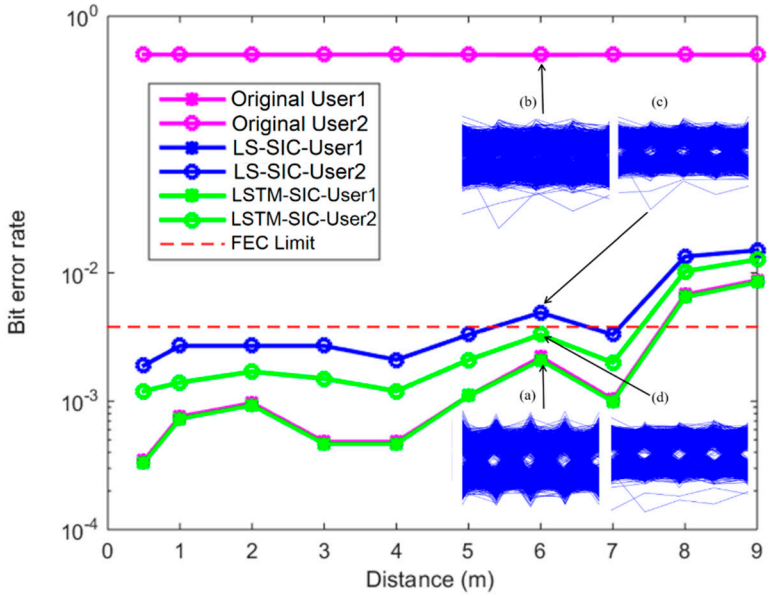


Figure 14. BERs at different distances with interference estimation optimization. Insets: eye diagrams of (**a**) the first user with equalization, (**b**) the second user with equalization, (**c**) the second user with LS-SIC, and (**d**) the second user with LSTM-SIC.

As shown in Figure 15, the BER performance of different interference reconstruction algorithms was further compared considering different power allocation ratios. It can be seen that when the power allocation of the two users changed, the BERs of both users decreased until the allocation ratio was 0.8. When the ratio was larger than 0.8, the BER of the original algorithm for the strong user (User 1) decreased sharply, and the BER of the weak user (User 2) deteriorated sharply and exceeded the FEC. The BER of User 1 reached a minimum value at the power allocation ratio of 0.95, which was lower than the FEC. After using the LS-SIC and the LSTM-SIC detection algorithms, both algorithms improved the BER of User 2 to satisfy the FEC limit for a power allocation ratio ranging between 0.8 and 0.97. As the power allocation ratio increased to 1, which is equivalent to single-user transmission, the BER became worse again. Therefore, the proposed algorithm can outperform the original SIC algorithm and significantly improve the BER performance of the weak user. It provides a viable solution to achieve successive interference cancellation detection of two users in free-space optical communications.

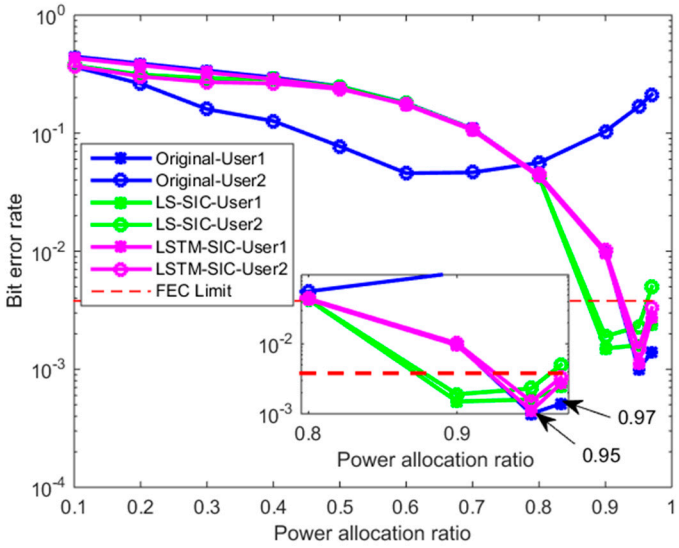


Figure 15. BERs under different power allocation ratios with interference estimation optimization.

As shown in Figure 16, the BER performance of the three successive interference estimation cancellation methods under different attenuation values was analyzed at a fixed power allocation ratio of 0.91. The BER of the original algorithm for User 1 was always below the FEC limit, and the BER of User 2 was below the FEC limit only when the attenuation value was 11 dB. After using LS-SIC and LSTM-SIC detection algorithms, the BERs of User 1 and User 2 were below the FEC limit, and the performance was close to the same.

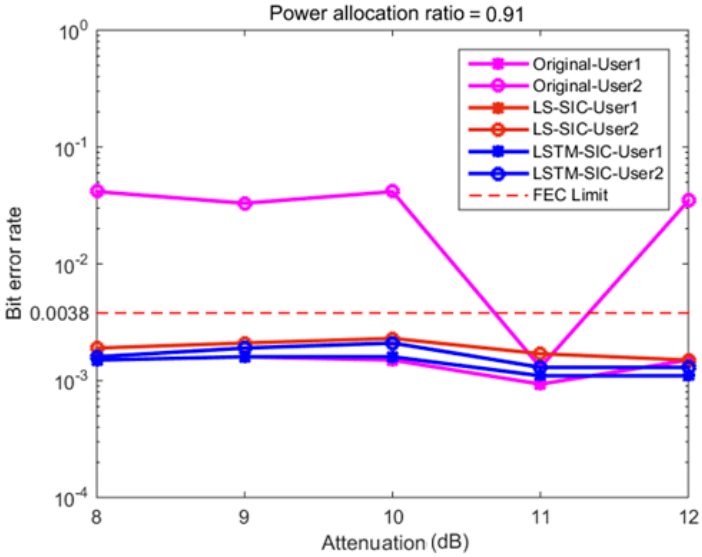


Figure 16. BERs at optimal power allocation ratio of 0.91 with interference estimation optimization.

As shown in Figure 17, the BER performance of the three successive interference estimation cancellation methods was analyzed for different attenuation values at a power allocation ratio of 0.92. The BER of the original algorithm for the strong user was always below the FEC limit, and the BER of the weak user was always above the FEC limit. After using LS-SIC and LSTM-SIC detection algorithms, the BERs of User 1 and User 2 were below the FEC limit, which shows that the final power allocation ratio has a greater effect on the BER performance.

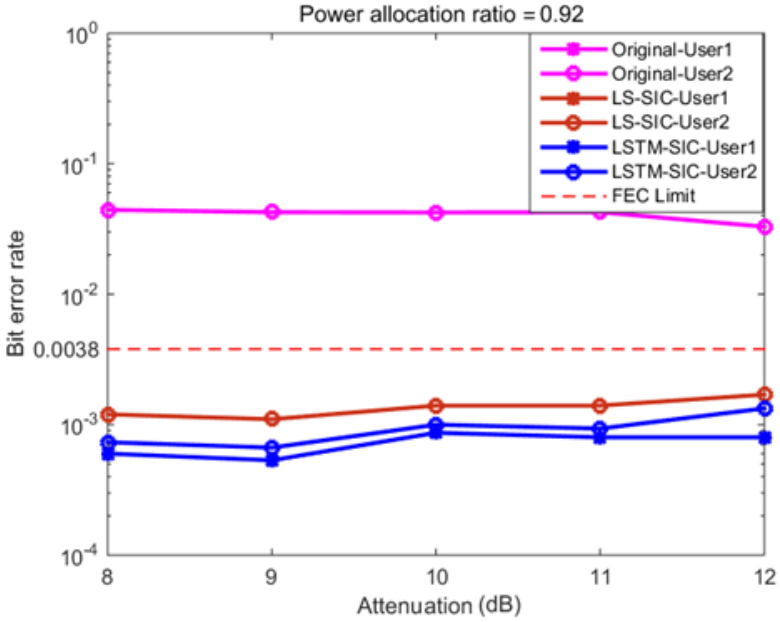


Figure 17. BERs at optimal power allocation ratio of 0.92 with interference estimation optimization.

As shown in Figure 18, the BER performance of the three successive interference estimation cancellation methods was analyzed for different attenuation values at a power allocation ratio of 0.93. The BER of the original algorithm for the strong user was always below the FEC limit, and the BER of the weak user decreased to the FEC limit with an attenuation value of 12 dB. After using LS-SIC and LSTM-SIC detection algorithms, both BERs of User 1 and User 2 were below the FEC limit. Since the power allocation ratio was 0.93, the power of the strong user was 0.93, while the power of the weak user was 0.07, and this ratio was suitable to demodulate both users accurately. An aggregate data rate up to 40 Mbps of the two signals on the same link could be achieved in the NOMA-VLC system. A comparison of the reported MISO VLC systems is given in Table 4.

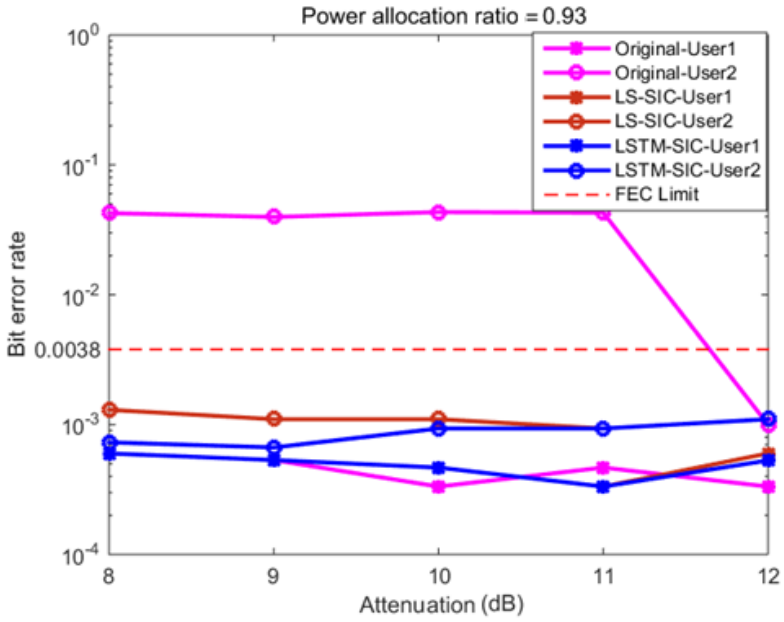


Figure 18. BERs at optimal power allocation ratio of 0.93 with interference estimation optimization.

Table 4. Luminescent concentrator-based MISO VLC systems reported in different works.

Reference	Materials	Light Source	Modulation Scheme	BER	Data Rate (Mbps)	Distance (m)
[17]	$CdZnSeS/ZnSe_{1.0}S_{1.3}$	QD blue μLEDs	NOMA	3.24×10^{-3}	120	1.5 underwater
[18]	Cm6 and DCM	Blue and green LEDs	OOK	4×10^{-3}	12	Not provided
[20]	Conjugated polymer	Blue LEDs	OFDM	<FEC	400	0.5 air
[22]	Cm6	White LEDs	OOK	<FEC	32	0.3 air
Our work	Material-1 (CdSe/ZnS)	Blue LD	NOMA	<FEC	40	1.5 air
Our work	Material-2 ($CsPbBr_3$-50)	Blue LD	NOMA	<FEC	40	1.5 air

5. Conclusions

In this work, we focus on indoor successive interference cancellation detection of optical uplink NOMA based on a fluorescent concentrator and downlink NOMA based on interference coefficient estimation. To investigate the performance of uplink NOMA, we consider fast-response fluorescent material to ensure a wide-coverage QD concentrator with an effective coverage area. Since NOMA has emerged as a promising candidate for practical band-limited multi-user VLC systems, our experiments demonstrate that the

high-speed MISO NOMA-VLC is suitable for free-space channel communication. The QD concentrator-empowered MISO NOMA-VLC system can support an aggregate data rate of 40 Mbps by 2 LDs over a 1.5 m free-space distance, which ensures a unique connectivity approach for indoor IoT applications. Furthermore, the LS-SIC and LSTM-SIC algorithms are proposed in the downlink NOMA communication system. We also propose a recurrent neural network-based guided frequency interference coefficient estimation algorithm in the NOMA-VLC communication system, which improves the accuracy of interference estimation by introducing interference coefficients. Numerical results demonstrate that our proposed algorithm is effective in providing more accurate reconstruction and in weakening the influence of error propagation. Using NOMA technology, the power multiplexing and rate doubling for two users with the same link is achieved. Interesting work to be further explored is to study the power multiplexing and interference detection algorithms in uplink and downlink NOMA to further enhance the system capacity. In the future, we will focus on improving the channel capacity with fast-response material. Furthermore, we will investigate the feasibility of the QD-based MISO-NOMA VLC system in an underwater environment. In addition, in future work, we would like to extend the two-user case to a multiple-user case for the MIMO-NOMA VLC system.

Author Contributions: Conceptualization, S.A.H.M. and Y.L.; methodology, S.A.H.M. and Y.L.; formal analysis, S.A.H.M., Y.L. and Z.Z.; investigation, S.A.H.M., Y.L., Z.Z. and A.A.; resources, Z.Z. and J.X.; data curation, Y.L., Z.Z. and A.A.; writing—original draft preparation, S.A.H.M., Y.L., Z.Z. and J.X.; writing—review and editing, S.A.H.M., Y.L., Z.Z., A.A. and J.X.; visualization, Y.L., Z.Z. and J.X.; supervision, J.X.; project administration, J.X.; funding acquisition, J.X. All authors have read and agreed to the published version of the manuscript.

Funding: Supported by the Science Foundation of Donghai Laboratory (DH-2022KF01015); the National Natural Science Foundation of China (NSFC) (61971378); the Strategic Priority Research Program of the Chinese Academy of Sciences (XDA22030208); and the Zhoushan-Zhejiang University Joint Research Project (2019C81081).

Institutional Review Board Statement: Not applicable.

Informed Consent Statement: Not applicable.

Data Availability Statement: Data underlying the results presented in this paper are not publicly available at this time but may be obtained from the authors upon reasonable request.

Conflicts of Interest: The authors declare no conflict of interest. The authors declare that they have no known competing financial interests or personal relationships that could have appeared to influence the work reported in this paper.

References

1. Chuang, Y.C.; Li, Z.Q.; Hsu, C.W.; Liu, Y.; Chow, C.W. Visible light communication and positioning using positioning cells and machine learning algorithms. *Opt. Express* **2019**, *27*, 16377–16383. [CrossRef] [PubMed]
2. Chow, C.W.; Liu, Y.; Yeh, C.H.; Chang, Y.H.; Lin, Y.S.; Hsu, K.L.; Liao, X.-L.; Lin, K.H. Display light panel and rolling shutter image sensor based optical camera communication (OCC) using frame-averaging background removal and neural network. *J. Light. Technol.* **2021**, *39*, 4360–4366. [CrossRef]
3. Mohsan, S.A.H. Optical camera communications: Practical constraints, applications, potential challenges, and future directions. *J. Opt. Technol.* **2021**, *88*, 729–741. [CrossRef]
4. Huang, X.H.; Lu, H.H.; Chang, P.S.; Liu, C.X.; Lin, Y.Y.; Ko, T.; Chen, Y.T. Bidirectional white-lighting WDM VLC–UWOC converged systems. *J. Light. Technol.* **2021**, *39*, 4351–4359. [CrossRef]
5. Tang, X.; Kumar, R.; Sun, C.; Zhang, L.; Chen, Z.; Jiang, R.; Wang, H.; Zhang, A. Towards underwater coherent optical wireless communications using a simplified detection scheme. *Opt. Express* **2021**, *29*, 19340–19351. [CrossRef]
6. Jiang, R.; Sun, C.; Zhang, L.; Tang, X.; Wang, H.; Zhang, A. Deep Learning Aided Signal Detection for SPAD-based Underwater Optical Wireless Communications. *IEEE Access* **2020**, *8*, 20363–20374. [CrossRef]
7. Zhang, L.; Tang, X.; Sun, C.; Chen, Z.; Li, Z.; Wang, H.; Jiang, R.; Shi, W.; Zhang, A. Over 10 attenuation length gigabits per second underwater wireless optical communication using a silicon photomultiplier (SiPM) based receiver. *Opt. Express* **2020**, *28*, 24968–24980. [CrossRef]
8. Lu, H.H.; Lin, Y.P.; Wu, P.Y.; Chen, C.Y.; Chen, M.C.; Jhang, T.W. A multiple-input-multiple-output visible light communication system based on VCSELs and spatial light modulators. *Opt. Express* **2014**, *22*, 3468–3474. [CrossRef] [PubMed]

9. Xu, G.; Zhang, N.; Xu, M.; Xu, Z.; Zhang, Q.; Song, Z. Outage Probability and Average BER of UAV-assisted Dual-hop FSO Communication with Amplify-and-Forward Relaying. *IEEE Trans. Veh. Technol.* **2023**, *23*, 4337. [CrossRef]
10. Li, C.Y.; Lu, H.H.; Tsai, W.S.; Feng, C.Y.; Chou, C.R.; Chen, Y.H.; Nainggolan, A. White-lighting and WDM-VLC system using transmission gratings and an engineered diffuser. *Opt. Lett.* **2020**, *45*, 6206–6209. [CrossRef]
11. Rahman, M.D.R.; Adedara, K.; Ashok, A. Enabling multiple access in visible light communication using liquid crystal displays: A proof-of-concept study. *Electronics* **2020**, *9*, 826. [CrossRef]
12. Qiu, Y.; Chen, H.; Li, J.; Meng, W. VLC-CDMA systems based on optical complementary codes. *IEEE Wirel. Commun.* **2020**, *27*, 147–153. [CrossRef]
13. Akhoundi, F.; Salehi, J.A.; Tashakori, A. Cellular underwater wireless optical CDMA network: Performance analysis and implementation concepts. *IEEE Trans. Commun.* **2015**, *63*, 882–891. [CrossRef]
14. Li, X.; Tong, Z.; Lyu, W.; Chen, X.; Yang, X.; Zhang, Y.; Liu, S.; Dai, Y.; Zhang, Z.; Guo, C.; et al. Underwater quasi-omnidirectional wireless optical communication based on perovskite quantum dots. *Opt. Express* **2022**, *30*, 1709–1722. [CrossRef] [PubMed]
15. Shi, J.; Hong, Y.; Deng, R.; He, J.; Chen, L.-K.; Chang, G.-K. Demonstration of real-time software reconfigurable dynamic power-and-subcarrier allocation scheme for OFDM-NOMA-based multi-user visible light communications. *J. Light. Technol.* **2019**, *37*, 4401–4409. [CrossRef]
16. Lin, B.; Ye, W.; Tang, X.; Ghassemlooy, Z. Experimental demonstration of bidirectional NOMA-OFDMA visible light communications. *Opt. Express* **2017**, *25*, 4348–4355. [CrossRef]
17. Wang, Z.; Zhang, L.; Li, J.; Wei, G.; Dong, Y.; Fu, H.Y. Fluorescent concentrator based MISO-NOMA for visible light communications. *Opt. Lett.* **2022**, *47*, 902–905. [CrossRef] [PubMed]
18. Manousiadis, P.P.; Chun, H.; Rajbhandari, S.; Vithanage, D.A.; Mulyawan, R.; Faulkner, G.; Haas, H.; O'Brien, D.C.; Collins, S.; Turnbull, G.A. Optical antennas for wavelength division multiplexing in visible light communications beyond the étendue limit. *Adv. Opt. Mater.* **2020**, *8*, 1901139. [CrossRef]
19. Manousiadis, P.P.; Rajbhandari, S.; Mulyawan, R.; Vithanage, D.A.; Chun, H.; Faulkner, G.; O'Brien, D.C.; Turnbull, G.A.; Collins, S.; Samuel, I.D.W. Wide field-of-view fluorescent antenna for visible light communications beyond the étendue limit. *Optica* **2016**, *3*, 702–706. [CrossRef]
20. Dong, Y.; Shi, M.; Yang, X.; Zeng, P.; Gong, J.; Zheng, S.; Zhang, M.; Liang, R.; Ou, Q.; Chi, N.; et al. Nanopatterned luminescent concentrators for visible light communications. *Opt. Express* **2017**, *25*, 21926–21934. [CrossRef]
21. Kang, C.H.; Dursun, I.; Liu, G.; Sinatra, L.; Sun, X.; Kong, M.; Pan, J.; Maity, P.; Ooi, E.N.; Ng, T.K.; et al. High-speed colour-converting photodetector with all-inorganic CsPbBr3 perovskite nanocrystals for ultraviolet light communication. *Light Sci. Appl.* **2019**, *8*, 94. [CrossRef] [PubMed]
22. Mulyawan, R.; Chun, H.; Gomez, A.; Rajbhandari, S.; Faulkner, G.; Manousiadis, P.P.; Vithanage, D.A.; Turnbull, G.A.; Samuel, I.D.; Collins, S.; et al. MIMO visible light communications using a wide field-of-view fluorescent concentrator. *IEEE Photonics Technol. Lett.* **2017**, *29*, 306–309. [CrossRef]
23. Wang, Z.; Yu, H.; Wang, D. Channel and bit adaptive power control strategy for uplink NOMA VLC systems. *Appl. Sci.* **2019**, *9*, 220. [CrossRef]
24. Dai, L.; Wang, B.; Yuan, Y.; Han, S.; Chih-Lin, I.; Wang, Z. Non-orthogonal multiple access for 5G: Solutions, challenges, opportunities, and future research trends. *IEEE Commun. Mag.* **2015**, *53*, 74–81. [CrossRef]
25. Tomida, S.; Higuchi, K. Non-orthogonal access with SIC in cellular downlink for user fairness enhancement. In Proceedings of the 2011 International Symposium on Intelligent Signal Processing and Communications Systems (ISPACS), Chiang Mai, Thailand, 7–9 December 2011; IEEE: Piscataway, NJ, USA, 2011; pp. 1–6.
26. Eroğlu, Y.S.; Yapıcı, Y.; Güvenç, I. Impact of random receiver orientation on visible light communications channel. *IEEE Trans. Commun.* **2018**, *67*, 1313–1325. [CrossRef]
27. Wang, J.Y.; Li, Q.L.; Zhu, J.X.; Wang, Y. Impact of receiver's tilted angle on channel capacity in VLCs. *Electron. Lett.* **2017**, *53*, 421–423. [CrossRef]
28. Soltani, M.D.; Purwita, A.A.; Zeng, Z.; Haas, H.; Safari, M. Modeling the random orientation of mobile devices: Measurement, analysis and LiFi use case. *IEEE Trans. Commun.* **2018**, *67*, 2157–2172. [CrossRef]
29. Soltani, M.D.; Wu, X.; Safari, M.; Haas, H. Access point selection in Li-Fi cellular networks with arbitrary receiver orientation. In Proceedings of the 2016 IEEE 27th Annual International Symposium on Personal, Indoor, and Mobile Radio Communications (PIMRC), Valencia, Spain, 4–8 September 2016; pp. 1–6.
30. Soltani, M.D.; Kazemi, H.; Safari, M.; Haas, H. Handover modeling for indoor Li-Fi cellular networks: The effects of receiver mobility and rotation. In Proceedings of the 2017 IEEE Wireless Communications and Networking Conference (WCNC), Francisco, CA, USA, 19–22 March 2017; pp. 1–6.
31. Eroğlu, Y.S.; Yapici, Y.; Güvenc, I. Effect of random vertical orientation for mobile users in visible light communication. In Proceedings of the 2017 51st Asilomar Conference on Signals, Systems, and Computers, Pacific Grove, CA, USA, 1–29 October 2017; pp. 238–242.
32. Wang, J.Y.; Wang, J.B.; Zhu, B.; Lin, M.; Wu, Y.; Wang, Y.; Chen, M. Improvement of BER performance by tilting receiver plane for indoor visible light communications with input-dependent noise. In Proceedings of the 2017 IEEE International Conference on Communications (ICC), Paris, France, 21–25 May 2017; pp. 1–6.

33. Guan, X.; Hong, Y.; Chan, C.C.K. Non-orthogonal multiple access with multicarrier precoding in visible light communications. In Proceedings of the 2016 21st Opto-Electronics and Communications Conference (OECC) Held Jointly with 2016 International Conference on Photonics in Switching (PS), Niigata, Japan, 3–7 July 2016; IEEE: Piscataway, NJ, USA, 2016; pp. 1–3.
34. Li, H.; Huang, Z.; Xiao, Y.; Zhan, S.; Ji, Y. Solution for error propagation in a NOMA-based VLC network: Symmetric superposition coding. *Opt. Express* **2017**, *25*, 29856–29863. [CrossRef]
35. Mounir, M.; El_Mashade, M.B.; Mohamed Aboshosha, A. On the selection of power allocation strategy in power domain non-orthogonal multiple access (PD-NOMA) for 6G and beyond. *Trans. Emerg. Telecommun. Technol.* **2022**, *33*, e4289. [CrossRef]
36. Jiang, R.; Sun, C.; Tang, X.; Zhang, L.; Wang, H.; Zhang, A. Joint User-Subcarrier Pairing and Power Allocation for Uplink ACO-OFDM-NOMA Underwater Visible Light Communication Systems. *J. Light. Technol.* **2021**, *39*, 1997–2007. [CrossRef]
37. Islam, S.M.; Zeng, M.; Dobre, O.A.; Kwak, K.S. Non-orthogonal multiple access (NOMA): How it meets 5G and beyond. *arXiv* **2019**, arXiv:1907.10001.
38. Chen, C.; Fu, S.; Jian, X.; Liu, M.; Deng, X.; Ding, Z. NOMA for energy-efficient LiFi-enabled bidirectional IoT communication. *IEEE Trans. Commun.* **2021**, *69*, 1693–1706. [CrossRef]
39. Sadat, H.; Abaza, M.; Mansour, A.; Alfalou, A. A survey of NOMA for VLC systems: Research challenges and future trends. *Sensors* **2022**, *22*, 1395. [CrossRef]
40. Marshoud, H.; Kapinas, V.M.; Karagiannidis, G.K.; Muhaidat, S. Non-orthogonal multiple access for visible light communications. *IEEE Photonics Technol. Lett.* **2015**, *28*, 51–54. [CrossRef]
41. Zhao, Q.; Jiang, J.; Wang, Y.; Du, J. A low complexity power allocation scheme for NOMA-based indoor VLC systems. *Opt. Commun.* **2020**, *463*, 125383. [CrossRef]
42. Chen, C.; Zhong, W.D.; Yang, H.; Du, P. On the performance of MIMO-NOMA-based visible light communication systems. *IEEE Photonics Technol. Lett.* **2017**, *30*, 307–310. [CrossRef]
43. Yang, Z.; Xu, W.; Li, Y. Fair non-orthogonal multiple access for visible light communication downlinks. *IEEE Wirel. Commun. Lett.* **2016**, *6*, 66–69. [CrossRef]
44. Tahira, Z.; Asif, H.M.; Khan, A.A.; Baig, S.; Mumtaz, S.; Al-Rubaye, S. Optimization of non-orthogonal multiple access based visible light communication systems. *IEEE Commun. Lett.* **2019**, *23*, 1365–1368. [CrossRef]
45. Eroglu, Y.S.; Anjinappa, C.K.; Guvenc, I.; Pala, N. Slow beam steering and NOMA for indoor multi-user visible light communications. *IEEE Trans. Mob. Comput.* **2019**, *20*, 1627–1641. [CrossRef]
46. Pham, Q.V.; Huynh-The, T.; Alazab, M.; Zhao, J.; Hwang, W.J. Sum-rate maximization for UAV-assisted visible light communications using NOMA: Swarm intelligence meets machine learning. *IEEE Internet Things J.* **2020**, *7*, 10375–10387. [CrossRef]
47. Zhang, X.; Gao, Q.; Gong, C.; Xu, Z. User grouping and power allocation for NOMA visible light communication multi-cell networks. *IEEE Commun. Lett.* **2016**, *21*, 777–780. [CrossRef]
48. Eltokhey, M.W.; Khalighi, M.A.; Ghazy, A.S.; Hranilovic, S. Hybrid NOMA and ZF pre-coding transmission for multi-cell VLC networks. *IEEE Open J. Commun. Soc.* **2020**, *1*, 513–526. [CrossRef]
49. Raj, R.; Dixit, A. An Energy-Efficient Power Allocation Scheme for NOMA-Based IoT Sensor Networks in 6G. *IEEE Sens. J.* **2022**, *22*, 7371–7384. [CrossRef]
50. Dogra, T.; Bharti, M.R. User pairing and power allocation strategies for downlink NOMA-based VLC systems: An overview. *AEU-Int. J. Electron. Commun.* **2022**, *149*, 154184. [CrossRef]
51. Fu, Y.; Hong, Y.; Chen, L.K.; Sung, C.W. Enhanced power allocation for sum rate maximization in OFDM-NOMA VLC systems. *IEEE Photonics Technol. Lett.* **2018**, *30*, 1218–1221. [CrossRef]
52. Feng, S.; Bai, T.; Hanzo, L. Joint power allocation for the multi-user NOMA-downlink in a power-line-fed VLC network. *IEEE Trans. Veh. Technol.* **2019**, *68*, 5185–5190. [CrossRef]
53. Feng, S.; Zhang, R.; Xu, W.; Hanzo, L. Multiple access design for ultra-dense VLC networks: Orthogonal vs non-orthogonal. *IEEE Trans. Commun.* **2018**, *67*, 2218–2232. [CrossRef]
54. Kusaladharma, S.; Zhu, W.-P.; Ajib, W.; Baduge, G.A.A. Rate and Energy Efficiency Improvements of Massive MIMO-Based Stochastic Cellular Networks with NOMA. *IEEE Trans. Green Commun. Netw.* **2021**, *5*, 1467–1481. [CrossRef]
55. Zeng, M.; Yadav, A.; Dobre, O.A.; Poor, H.V. Energy-Efficient Power Allocation for MIMO-NOMA with Multiple Users in a Cluster. *IEEE Access* **2018**, *6*, 5170–5181. [CrossRef]
56. Yang, Z.; Ding, Z.; Fan, P.; Al-Dhahir, N. A General Power Allocation Scheme to Guarantee Quality of Service in Downlink and Uplink NOMA Systems. *IEEE Trans. Wirel. Commun.* **2016**, *15*, 7244–7257. [CrossRef]
57. Yang, Z.; Xu, W.; Pan, C.; Pan, Y.; Chen, M. On the Optimality of Power Allocation for NOMA Downlinks with Individual QoS Constraints. *IEEE Commun. Lett.* **2017**, *21*, 1649–1652. [CrossRef]
58. Li, S.; Dang, X.; Xu, G.; Yu, X.; Hao, C.; Li, J. Detection of Downlink Asynchronous NOMA with MSK-Type Signals. *IEEE Commun. Lett.* **2023**, *27*, 1442–1446. [CrossRef]
59. Jamali, M.V.; Mahdavifar, H. Uplink non-orthogonal multiple access over mixed RF-FSO systems. *IEEE Trans. Wirel. Commun.* **2020**, *19*, 3558–3574. [CrossRef]
60. Zhang, J.; Zhang, L.; Pan, G. Outage Performance for NOMA-based FSO-RF Systems with a Dual Energy Harvesting Mode. *IEEE Internet Things J.* **2023**. [CrossRef]
61. Obeed, M.; Dahrouj, H.; Salhab, A.M.; Zummo, S.A.; Alouini, M.-S. User Pairing, Link Selection, and Power Allocation for Cooperative NOMA Hybrid VLC/RF Systems. *IEEE Trans. Wirel. Commun.* **2021**, *20*, 1785–1800. [CrossRef]

62. Raj, R.; Dixit, A. Outage Analysis and Reliability Enhancement of Hybrid VLC-RF Networks Using Cooperative Non-Orthogonal Multiple Access. *IEEE Trans. Netw. Serv. Manag.* **2021**, *18*, 4685–4696. [CrossRef]
63. Almohimmah, E.M.; Alresheedi, M.T. Error analysis of NOMA-based VLC systems with higher order modulation schemes. *IEEE Access* **2019**, *8*, 2792–2803. [CrossRef]
64. Ren, H.; Wang, Z.; Du, S.; He, Y.; Chen, J.; Han, S.; Yu, C.; Xu, C.; Yu, J. Performance improvement of NOMA visible light communication system by adjusting superposition constellation: A convex optimization approach. *Opt. Express* **2018**, *26*, 29796–29806. [CrossRef]
65. Dong, Z.; Shang, T.; Li, Q.; Tang, T. Differential evolution-based optimal power allocation scheme for NOMA-VLC systems. *Opt. Express* **2020**, *28*, 21627–21640. [CrossRef]
66. Wang, G.; Shao, Y.; Chen, L.K.; Zhao, J. Improved joint subcarrier and power allocation to enhance the throughputs and user fairness in indoor OFDM-NOMA VLC systems. *Opt. Express* **2021**, *29*, 29242–29256. [CrossRef]
67. Song, X.; Liu, Y.; Xue, L.; Wang, J.; Zhang, J.; Wang, J.; Jiang, L.; Cheng, Z. Time-series well performance prediction based on Long Short-Term Memory (LSTM) neural network model. *J. Pet. Sci. Eng.* **2020**, *186*, 106682. [CrossRef]
68. Bin, T.; Wang, G.; Xu, Z.; Zhang, Y.; Zhao, X. Communication delay compensation for string stability of CACC system using LSTM prediction. *Veh. Commun.* **2021**, *29*, 100333.
69. Sherstinsky, A. Fundamentals of recurrent neural network (RNN) and long short-term memory (LSTM) network. *Phys. D Nonlinear Phenom.* **2020**, *404*, 132306. [CrossRef]

Disclaimer/Publisher's Note: The statements, opinions and data contained in all publications are solely those of the individual author(s) and contributor(s) and not of MDPI and/or the editor(s). MDPI and/or the editor(s) disclaim responsibility for any injury to people or property resulting from any ideas, methods, instructions or products referred to in the content.